



Upscaling polydispersed particle transport in porous media using pore network model

Jongmuk Won¹ · Junghwoon Lee² · Susan E. Burns²

Received: 4 July 2019 / Accepted: 14 July 2020 / Published online: 23 July 2020
 © Springer-Verlag GmbH Germany, part of Springer Nature 2020

Abstract

Understanding particle transport in porous media is critical in the sustainability of many geotechnical and geoenvironmental infrastructure. To date, the determination of the first-order rate coefficients in the advection–dispersion equation for simulating attachment and detachment of particles in saturated porous media typically has been relied on the result of laboratory-scale experiments. However, to determine attachment and detachment coefficients under varied hydraulic and geochemical variables, this method requires a large experimental matrix because each test provides only one set of attachment and detachment coefficients. The work performed in this study developed a framework to upscale the results obtained in pore-scale modeling to the continuum scale through the use of a pore network model. The developed pore network model incorporated variables of mean particle size, the standard deviation of particle size distribution, and interparticle forces between particles and sand grains. The obtained retention profiles using the pore network model were converted into attachment coefficients in the advection–dispersion equation for long-term and large-scale simulation. Additionally, by tracking individual particles during and after the simulation, the pore network model introduced in this study can also be employed for modeling the clogging phenomenon, as well as fundamental investigation of the impact of particle size distribution on particle retention in the sand medium.

Keywords First-order coefficient · Particle size distribution · Particle transport · Pore network · Upscaling

List of symbols

A ($M L^2 T^{-1}$)	Hamaker constant	g_t, g_p ($M^{-1} L^4 T$)	Hydraulic conductances of throats and the half of pores
C_0, C ($M L^{-3}$)	Inlet concentration and particle concentration	h_0 (L)	Minimum separation distance
d_{50} (L)	Median grain size of sand	i, j	Pore index
D_{ij} (L)	The Euclidean distance between centers of pore i and j	J_T ($M L^{-3} T^{-1}$)	Total particle flux
d_p, d_t (L)	Diameter of the pore and throats	k ($L T^{-1}$)	Hydraulic conductivity
		k_{att}, k_{det} (T^{-1})	First-order coefficients for attachment and detachment
		K_1	Pore wall correction factor
		L_{ij} (L)	The length of the throat between pore i and pore j
		L_{ref} (L)	Reference length
		M_{ij} (M)	Transferred mass of particles from pore i to pore j
		n	Porosity
		N_c	Total number of sampled particles
		P ($M L T^{-2}$)	Pressures at pores
		p_{cap}	Capture probability
		p_m	Cumulative probability of m th interval
		Q_{ij} ($L^3 T^{-1}$)	The flow rate between pore i and j
		r_c, r_t (L)	Radius of particle and throat
		r_{new} (L)	Updated effective throat radius

Electronic supplementary material The online version of this article (<https://doi.org/10.1007/s11440-020-01038-z>) contains supplementary material, which is available to authorized users.

✉ Jongmuk Won
 jmwon@ulsan.ac.kr; whdanr1111@gmail.com

¹ Department of Civil and Environmental Engineering, University of Ulsan, Daehak-ro 93, Nam-gu, Ulsan 680-749, South Korea

² School of Civil and Environmental Engineering, Georgia Institute of Technology, 790 Atlantic Drive, N.W., Atlanta, GA 30332-0355, USA

r_p (L)	Radius of pores
S_{att}, S_{max} ($M M^{-1}$)	Solid phase attached particles and attachment capacity
$t, \Delta t$ (T)	Time and time for one time step
U ($L T^{-1}$)	Centerline velocity of throats
v, v_c ($L T^{-1}$)	Velocity of water and critical velocity
V_{inlet} (L^3)	Total volume of inlet pores
$\Delta P_p, \Delta P_{total}$ ($M L T^{-2}$)	Pressure drop at a throat and total pressure drop
θ, θ_0	Lumped parameter and interparticle force parameter
M ($M L^{-1} T^{-1}$)	Viscosity of water
μ_c, σ_c	Mean and standard deviation of particle size distribution
ρ_s, ρ_b ($M L^{-3}$)	Density of particle and bulk density of sand
ψ_{att}	Attachment function

1 Introduction

Understanding particle transport in porous media is critical in many engineering problems. For example, suffusion can be defined as a detachment of fine particles induced by hydrodynamic forces applied to the attached fine particles [12, 21, 22, 26]. It has been reported by previous studies for investigating the stability of dams because the seepage-induced detachment and transport of fine particles may cause significant deformation of dams [16, 21, 25]. In addition, retention or detachment of fine particles alters the hydraulic conductivity of coarse-grained soils, which imply that particle transport is critical in the performance of flow-related geotechnical infrastructure [33, 35].

Particles that are transporting through a saturated soil medium can be retained through straining and attachment due to large sizes of particles and attractive interparticle forces or can be detached through hydrodynamic forces. In continuum scale, most studies on investigating particles transporting through the soil, filters, or any geologic media will typically use two or three rate coefficients with advection and dispersion terms to account for mechanisms associated with particle retention or detachment. For example, some studies used attachment and detachment coefficients [7, 15], reversible and irreversible retention of particles with three rate coefficients [8] or straining, attachment, and detachment of particles [4]. In some cases, as many as five rate coefficients have been used to model particle retention at kinetic and equilibrium sites [30]. These modified advection–dispersion-type equations are well suited to explain and fit experimental data obtained in

the laboratory for any combination of particle type and porous media. In order to model the retention of particles through saturated porous media and predict the reduction in hydraulic conductivity, it is common practice to use laboratory-measured values of particle transport for determining first-order rate coefficients (attachment or detachment) in the advection–dispersion equation [4].

While laboratory-scale experimental results provide the data (usually retention profiles or breakthrough curves) for evaluating the first-order rate coefficient, it is typically not possible to express those coefficients as a function of the pore size distribution of the porous media, the particle size distribution of the particles, and other microscale parameters such as dead pore in water flow. This implies that a single experiment produces one set of back-calculated rate coefficients, which are only valid for corresponding experimental conditions. Therefore, a large experimental matrix would be required to obtain the first-order coefficients at varied size ratios (particle/filtration medium) or different hydrogeochemical conditions (pH, ionic strength, and flow rate) for large-scale simulation of particle transport.

Consequently, it is beneficial to develop an upscaling methodology that can reduce the experimental effort by incorporating the impact of the above-mentioned factors that influence particle retention. Pore network models are computationally less expensive than other pore-scale simulations such as the lattice Boltzmann method and smoothed particle hydrodynamics [27, 34], and they improve on the disadvantages of a macroscopic volume-averaged continuum-scale model (advection–dispersion equation with first-order rate coefficients). The ability to incorporate microscopic features of porous media, as well as properties of the transporting particles, is the main advantages of using pore network models for simulating particle transport in porous media. While it is computationally expensive, pore network models also allow tracking of individual particles during transport and can determine the representative volume of porous media for particle transport within a particular pore size distribution.

This work developed a framework to evaluate attachment coefficients from retention profiles obtained by the pore network model under varied particle size distribution and median size: upscaling from the pore scale to the continuum scale. A three-dimensional cubic pore network was constructed, and particle size distributions of kaolinite particles at three ionic strengths were used to obtain mean and standard deviation values to describe the particle size distribution of the particle. In addition, the impact of the mean and standard deviation of distributions on the retention profiles, breakthrough curves, and the reduction in hydraulic conductivity were examined.

2 Model formulation

2.1 Background: network construction and quantification of fluid flow

The network model was constructed using the open-source project code OpenPNM, which is written in Python. OpenPNM was developed to simulate multiphase flow in porous media [1, 11, 31]. A three-dimensional simple cubic network was constructed to represent the sand medium, which was used for the efficiency of computational work and the effective description of the transport process (easily be obtained through coordination number) [17, 29]. Since all simulations were performed for the case of kaolinite particles transporting through the silica sand, all material-related properties of particles and sand used in pore network simulation were equivalent to kaolinite and Ottawa 20/30 sand.

Because the main purpose of this study was to develop the framework of upscaling the particle transport from the pore scale to continuum scale, the pore network model representing the geometry of the sand medium is not considered here as it requires information on the pore structure of the sand medium (i.e., pore size distribution or X-ray CT image), which may limit the application of the framework. Furthermore, the θ_0 value [Eq. (10)] introduced in Sect. 2.3 can be determined by experimental results regardless of types of the pore network model. Therefore, a cubic network model was used to represent the sand medium for this particular application presented in this paper.

In order to more closely emulate Ottawa 20/30 sand packing, the network was modeled using a coordination number (CN) ranging from 5.4–5.5 in all simulations, which was created by randomly eliminating throats from the regular three-dimensional cubic network (CN = 6 for cubic network) [32]. The distance between centers of pores in the network was set equal to the median grain size of the sand (d_{50}), which is equivalent to the throat length of the pore network for uniform sand, based on the geometry of the discrete element model as described in [37]. The shapes of the pores and throats were assumed to be spheres and cylinders, respectively, and the diameters of the pores were initially determined at a given distribution, with the length of throats evaluated as:

$$L_{ij} = D_{ij} - (d_{p(i)} - d_{p(j)})/2 \quad (1)$$

Because all particle transport simulations in this work were performed in the saturated condition, only single-phase flow was taken into account for the flow calculation in the network model. The Hagen–Poiseuille equation was used for calculating single-phase flow in a cylindrical tube

[9], where the hydraulic conductances of throats and half of the pores are expressed as:

$$g_t = \frac{\pi d_t^4}{128L\mu} \quad (2)$$

$$g_p = \frac{\pi d_p^4}{128r_p\mu} \quad (3)$$

Using Eqs. (2) and (3), the hydraulic conductance of fluid between pore i and j (g_{ij}) can be obtained by the harmonic mean of three hydraulic conductances:

$$g_{ij} = \left(\frac{1}{g_{p(i)}} + \frac{1}{g_t} + \frac{1}{g_{p(j)}} \right)^{-1} \quad (4)$$

The flow rate between pore i and j (Q_{ij}) is obtained successively according to:

$$Q_{ij} = g_{ij}(P_i - P_j) \quad (5)$$

Pressure values of each pore at given boundary conditions can be determined by solving a system of linear equations based on the mass conservation of fluid at all pores except the boundary pores. To simulate fluid flow from inflow to outflow, Dirichlet-type boundary conditions (pressure difference corresponding to the hydraulic gradient of 0.71) were applied at the top and bottom pores for the calibration of hydraulic conductivity (shown later) before injecting particles into the network. During particle injection, Neumann-type boundary conditions (flow rate was $0.175 \text{ cm}^3 \text{ s}^{-1}$, which corresponds to Darcy velocity of 0.2 cm s^{-1}) were applied at the outflow pores to evaluate the reduction in hydraulic conductivity (k) due to particle retention under the constant flow rate. Particle retention decreased the throat diameter (d_t) in Eq. (2), and the hydraulic conductivity of the network in each time step was evaluated using Darcy's equation from the total pressure drop of the model.

The OpenPNM model was used to construct the pore network model and simulate water flow at a given pressure drop. The original contributions of this work for simulating particle transport can be summarized as follows: (1) generated particles at given particle size distribution to introduce to the model, (2) incorporated theoretical equations for retention of particles into the pore network model, (3) simulated the reduction in hydraulic conductivity, and (4) formatted the large set of data to evaluate particle size distributions of retained and transported particles.

2.2 Particle mass transport: development of sampling methodology

In all simulations, particles were injected at the inflow pores with a constant mass-based concentration. Consequently, the number of particles at the inflow pores, equivalent to the inlet concentration, was determined

through unit conversion using the volume and the density of particles, assuming that particles are a sphere. Assuming that the particle size distribution is well described by the lognormal distribution curve, the total number of sampled particles (N_c) is obtained by:

$$N_c = \frac{V_{\text{inlet}} C_0}{4/3\pi\rho_s \exp(3\mu_c + 4.5\sigma_c)} \quad (6)$$

Note that $\exp(3\mu_c + 4.5\sigma_c)$ in Eq. (6) is the expected value of r_c^3 in a lognormal distribution (the 3rd raw moment). After determining N_c , Latin hypercube sampling, one of the sampling techniques without replacement, was applied at the given particle size distribution. Application of Latin hypercube sampling enabled the sampled r_c to more accurately reflect the given particle size distribution regardless of N_c . The cumulative probability of the m th interval (P_m) by Latin hypercube sampling is given as:

$$p_m = \left(\frac{1}{N_c}\right)u_m + \left(\frac{m-1}{N_c}\right) \quad (7)$$

Using Eq. (7), m sampled r_c corresponding to p_m values can be obtained by inverting the cumulative distribution function. Note that u_m is fixed at 0.5 in all simulations to assure reproducibility of sampled r_c at given particle size distribution and to eliminate the randomness of sampling for the validity of N_c in Eq. (6). A periodic boundary condition was applied at the inflow pores for the injection of particles, and particles were tracked individually during their transport through the network.

2.3 Particle mass transfer: throat length and deposition

The transport of generated particles from pore to pore was obtained based on the corresponding mass transfer between pores in each time step, with the length of the pore throat included explicitly. The amount of transferred mass from pore i to adjacent pores was calculated using flow rate (Q_{ij}) through the corresponding pore throats coupled with a scaled reference length (L_{ref}) to eliminate the error associated with a mass transfer at the pore scale according to:

$$M_{ij} = C_i Q_{ij} \Delta t \left(\frac{L_{ij}}{L_{\text{ref}}}\right) \quad (8)$$

Here, M_{ij} is independent of L_{ij} at given Δt with an absence of (L_{ref}/L_{ij}) in Eq. (8). Note that Eq. (8) is valid for

pores adjacent to pore i only when $P_i > P_j$ (pore j can be multiple pores). By applying M_{ij} , the number of particles moving from pore i to pore j in each time step was determined through unit conversion. Using Q_{ij} in Eq. (8) means that the prediction of the particle movement was analogous to the flow-biased probability model presented in [36], which described the walking direction of particles based on the magnitude of flow rates at the neighboring throats.

Particles were considered retained in the throats if a random number between 0 and 1 for each particle was less than the capture probability (p_{cap}), which is expressed as [13, 28]:

$$p_{\text{cap}} = 4 \left[\left(\frac{\theta r_c}{r_t}\right)^2 - \left(\frac{\theta r_c}{r_t}\right)^3 \right] + \left(\frac{\theta r_c}{r_t}\right)^4 \quad (9)$$

To take the effect of water velocity at throats (v) into account, the lumped parameter, θ , is expressed as:

$$\theta = \theta_0 \exp(-v/v_c) \quad (10)$$

Analytically, v_c is given by [23]:

$$v_c = \frac{A}{61.218\pi\mu h_0^2} \quad (11)$$

The Hamaker constant ($= 9.36 \times 10^{-21}$ J) in silica sand–water–kaolinite system was used in all simulations, which was calculated by refractive indexes and dielectric constants of those materials [18]. In addition, the interaction energy between sand and kaolinite was evaluated based on the Derjaguin–Landau–Verwey–Overbeek (DLVO) theory. The result of the DLVO calculation (Fig. S1 in Supplementary material) revealed that a high energy barrier between sand and kaolinite particles hindered the attachment of particles at the primary minimum, which resulted in the primary attachment at a secondary minimum [5, 19, 20]. Therefore, h_0 was set equal to the separation distance corresponding to the secondary minimum ($= 5.2$ nm). As a result, v_c remained constant ($= 1.8 \times 10^{-3}$ m s⁻¹) throughout the simulation.

The retention of particles decreased the radius of throats and increased the pressure drop within the network. The pressure drop at a throat (ΔP_p) due to the retention of particles is determined as [14]:

$$\Delta P_p = \frac{12\mu r_c U}{r_t^2} \left(1 - \left(1 - \frac{r_c}{r_t} \right)^2 \right)^2 K_1 \quad (12)$$

$$K_1 = \frac{1 - (2/3)(r_c/r_t)^2 - 0.202(r_c/r_t)^5}{1 - 2.105(r_c/r_t) + 2.086(r_c/r_t)^3 - 1.707(r_c/r_t)^5 + 0.726(r_c/r_t)^6} \quad (13)$$

where U is $2 \cdot v$ for laminar pipe flow. The total pressure drop (ΔP_{total}) of the throat can be obtained by $\Delta P_{\text{total}} = \Delta P_{\text{throat}} + \sum \Delta P_p$. The updated effective throat radius (r_{new}) for the calculation in the next time step after N particles were retained is determined by [28]:

$$\frac{1}{r_{\text{new}}^4} = \frac{1}{r_t^4} + \frac{0.75}{r_t^4} \sum_{i=1}^N \frac{r_c}{L} \left(1 - \left(1 - \frac{r_c}{r_t} \right)^2 \right)^2 K_1 \quad (14)$$

Note that the retention of particles only occurred in network throats, indicating that the radius of the pores remained constant. In addition, θ decreased as the amount of retained particles increased under constant flow rate due to the increase in v (r_t decreases as particles retained). A flowchart of key features used for predicting particle transport/retention is illustrated in Fig. 1.

2.4 Continuum equation for particle transport

The macroscale model used in this work for describing particle transport was an advection–dispersion equation with two first-order coefficients to account for the attachment and detachment of particles [7]:

$$\frac{\partial(nC)}{\partial t} = -\nabla \cdot J_T - nk_{\text{att}}\psi_{\text{att}}C + \rho_b k_{\text{det}}S_{\text{att}} \quad (15)$$

where J_T is the sum of advective and dispersive fluxes and dispersion coefficient of the particle was calculated by given Reynolds number and Péclet number [10] and $\psi_{\text{att}} = (1 - S_{\text{att}})/S_{\text{max}}$.

Optimization analysis was performed using the trust-region algorithm to yield optimized first-order attachment and detachment coefficients at a given retention profile

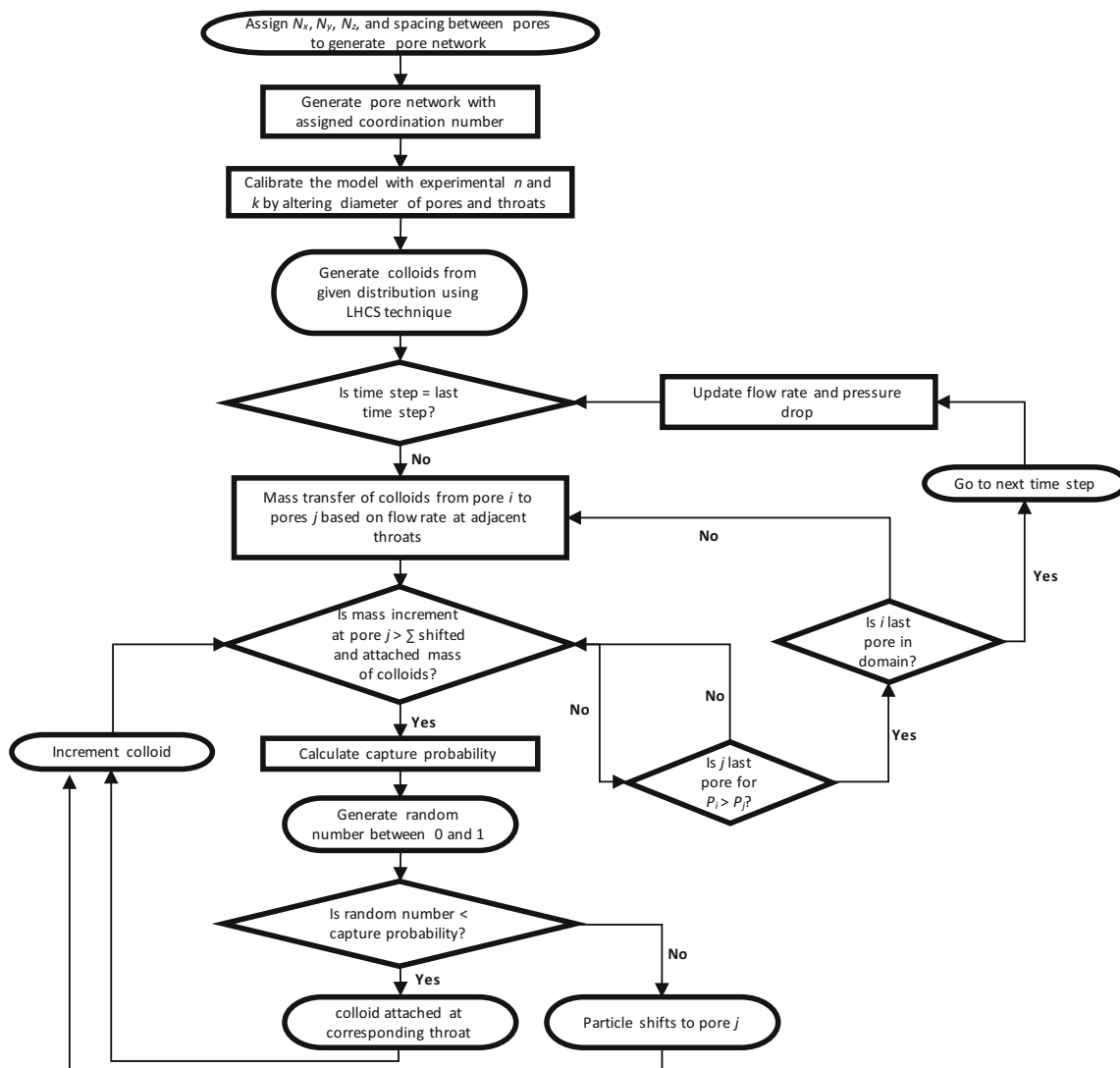


Fig. 1 Flowchart describing key features of the model

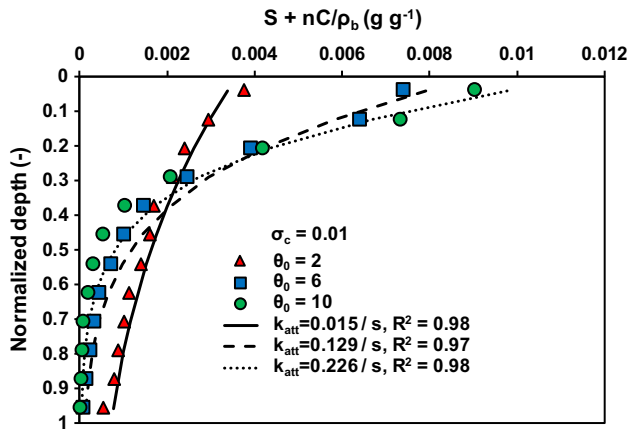


Fig. 2 Examples of optimization analysis: Markers represent the results from pore network simulation, and lines represent the best-fit curves by solving continuum equation [Eq. (15)]

(RP) obtained by the pore network model (least square sense as illustrated in Fig. 2). The implicit finite difference method was used to solve Eq. (15) with convergence in each time step. The straining mechanism, which is defined as particle immobilization due to narrow throat sizes [2, 6], was incorporated into the attachment coefficient in Eq. (15). This allowed the use of a single coefficient, k_{att} , to model retention as a function of the input parameters including particle size distribution, the median size of the particle, and throat size distribution.

2.5 Model calibration and determination of the size of the model

The model was calibrated using the value of the experimentally measured hydraulic conductivity for Ottawa 20/30 sand (0.14 cm s^{-1}) by altering the aspect ratio between pores and throats (diameter of pores/diameter of

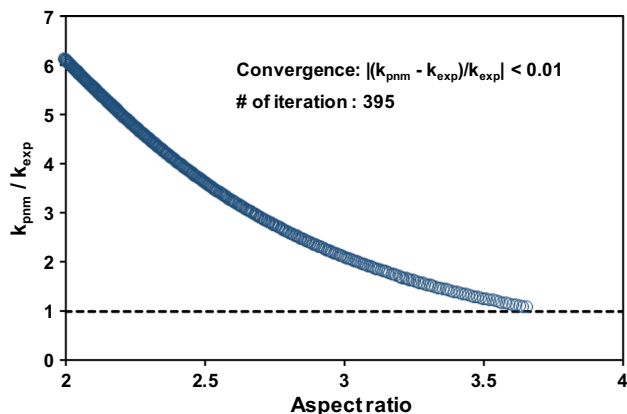


Fig. 3 Calibration of the hydraulic conductivity of the network (k_{pnm}) to experimentally measured hydraulic conductivity (k_{exp})

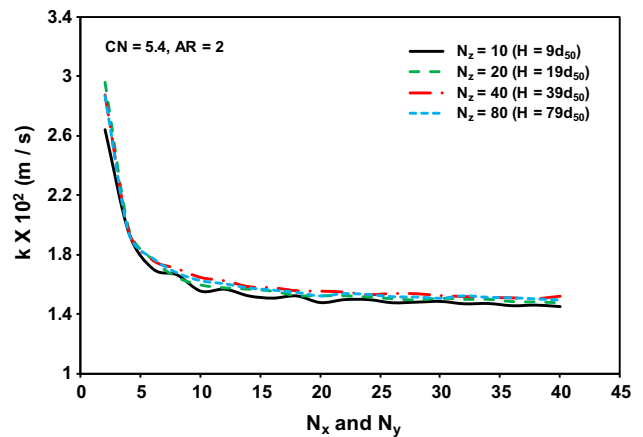


Fig. 4 The effect of numbers of pores in x -, y -, and z -axes (N_x , N_y , and N_z) on the hydraulic conductivity (k) of the network. Note that $N_x = N_y$ in this calculation

throats) until the hydraulic conductivity of pore network model converged to the measured hydraulic conductivity (Fig. 3). In addition, in order to avoid boundary effects, the number of modeled pores in the x -, y -, and z -axes was determined as 14, 14, and 40 (Fig. 4). By performing this calibration, the cubic pore network used in this work is hydraulically consistent with the real sand medium. An example visualization of the pore network is illustrated in Fig. 5.

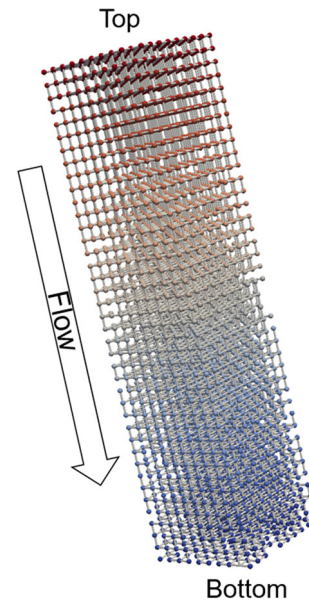


Fig. 5 An example visualization of the regular cubic pore network used in this simulation. Colloid suspension was injected at the top of the network, and part of throats were eliminated randomly until $CN \sim 5.4$. The color of pores indicates pressure values at pores from high (colored in red) to low (colored in blue) (color figure online)

Table 1 Properties of kaolinite and sand used in the simulation

Property	Median radius (μm)	μ_c	σ_c	Note
Kaolinite	3.7, 6, 9 ^a	1.3, 1.8, 2.2	0.01, 0.1, 0.2, 0.3	PSD fitted to lognormal distribution
Sand	360	–	–	Set to the distance between centers of pores

^aRefer to Fig. S2 and PSD: particle size distribution

2.6 Simulation cases

In total, 72 simulations were performed with the following values for the control variables: mean particle size (μ_c) = 1.3, 1.8, and 2.2, standard deviation of particle size (σ_c) = 0.01, 0.1, 0.2, and 0.3, and lumped interparticle force parameter (θ_0) = 2, 4, 6, 8, 10, and 12. The mean (μ_c) values used in the simulation corresponded to the experimental median sizes of kaolinite particles presented in Fig. S2. Retention profiles, breakthrough curves, the reduction in hydraulic conductivity, and size distribution of particles in the retention profiles and the breakthrough curves were evaluated for the 72 cases, with the mass-based concentration C_0 in Eq. (6) fixed at 1 g L^{-1} in all simulations. Note that the sizes of kaolinite particle used here represent the size of kaolinite clusters (aggregated formation of kaolinite particles), which implies that the proposed framework in this work can apply to most of the colloidal particle transport (particles $< 10 \mu\text{m}$ can be defined as colloidal particles [24]). The properties used in this study are summarized in Table 1.

3 Results and discussion

3.1 Retention profiles and evaluating attachment coefficients

The retention profiles of 72 cases obtained by the pore network model (some cases are presented in Fig. 6) were fitted in order to determine the attachment coefficient (k_{att}) in Eq. (15) (Fig. 2), which can be used in macroscale simulation (Fig. 7). The value of k_{det} was fixed to $1 \times 10^{-4}/\text{s}$, by assuming that the detachment coefficient of particles was proportional to the flow rate which was constant in all simulation in this work, and to allow quantitative comparison of k_{att} between each condition. As illustrated in Fig. 7, it is apparent that k_{att} increased as θ_0 increased due to the increase in capture probability. In addition, under constant interaction energy (θ_0), k_{att} increased as μ_c and σ_c increased because increases in the median particle size and in the standard deviation of the particle size resulted in higher capture probability at the column inlet. Physically, θ_0 represents the interaction

energy between particles and the sand grain, with increasing θ_0 values indicating higher attractive energy (i.e., more favorable attachment). In addition, because θ_0 is a single parameter that represents both straining and attachment deposition mechanisms, increasing the value of θ_0 indicates a high chance for particles to also be retained by straining (reflected in increasing μ_c and σ_c). For clay particle transport/retention in a sand medium, large values of θ_0 represent the solution chemistry of low ionic strength, which results in more exponential retention profiles due to the large sizes of clay clusters that form in solutions with low electrolyte concentrations [33]. Note that attractive energy between particles and a porous media matrix is a function of mineralogy and solution chemistry.

The above-mentioned upscaling framework provides the evaluation of k_{att} for the particular particle–porous media system under conditions of variable flow rate and particle sizes (particle and sand), all of which can be evaluated from one experimental retention profile. Because all parameters used in the pore network model except θ_0 are available from experimental conditions, θ_0 can be back-calculated based on the observed experimental retention profile. (θ_0 is not dependent on particle sizes and hydrological conditions.) Using this back-calculated θ_0 allows determination of retention profiles at different sizes of particles and pores, as well as a range of hydrological conditions [Eqs. (10), (11)] in the pore network model, which will eventually provide k_{att} at different conditions at given particle–sand medium system for long-term and large-scale simulation. The limitation of not being able to take particle size distribution and hydrological conditions into account in the continuum scale model [Eq. (15)] can be resolved using the proposed framework.

3.2 Effect of parameter θ_0 and particle size distribution of clay particle (μ_c and σ_c)

The breakthrough curves and reduction in hydraulic conductivity at varied θ_0 , μ_c , and σ_c are presented in Fig. 8. An increase in θ_0 resulted in a larger mass of retained particles which lowered particle breakthrough (C/C_0) and reduced hydraulic conductivity (K/K_0) during 10 pore volumes of flow (Fig. 8), as was anticipated. Essentially no particle

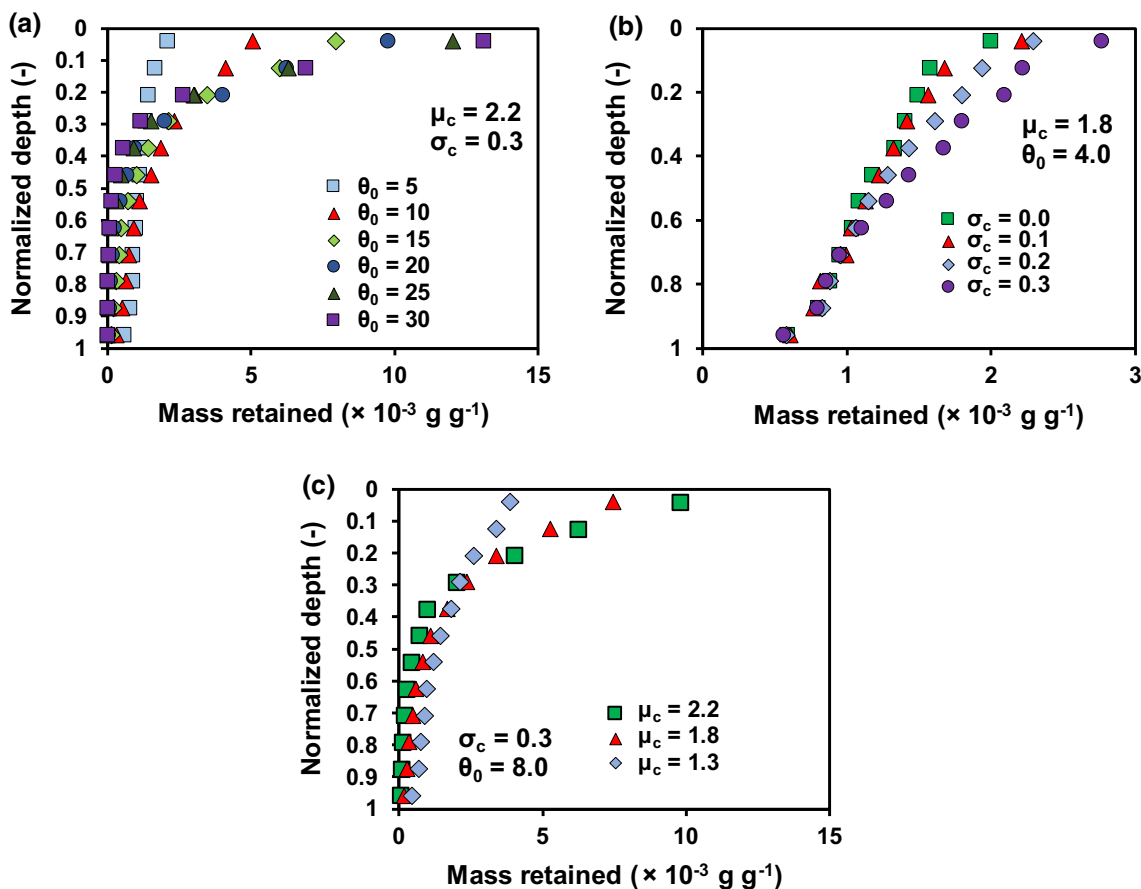


Fig. 6 Retention profiles under a varied θ_0 at $\mu_c = 2.2$ and $\sigma_c = 0.3$, b varied σ_c at $\mu_c = 1.8$ and $\theta_0 = 4$, c under varied $\mu_c = 2.2, 1.8$ and 1.3 at $\theta_0 = 8$ and $\sigma_c = 0.3$ (c). $S + n \cdot Cl\rho_b$ represents retained particles in the solid phase (S) and aqueous phase ($n \cdot Cl\rho_b$)

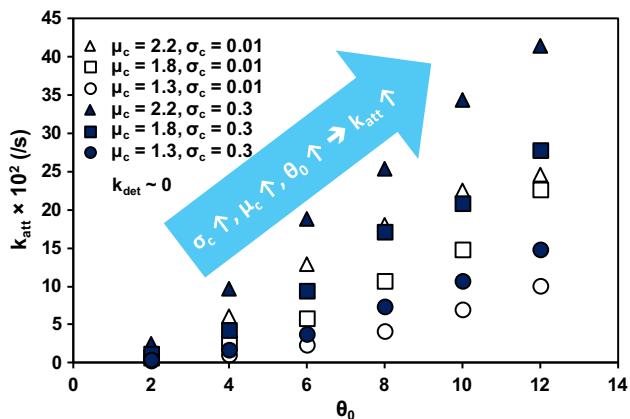


Fig. 7 Optimized k_{att} under varied θ_0 at $\mu_c = 2.2, 1.8, 1.3$ and $\sigma_c = 0.01, 0.3$. Increasing interparticle attraction, particle size, and particle size standard deviation increased the capture probability, resulting in increased k_{att} (raw data are summarized in Table S1 in supplementary material)

breakthrough was observed at values of $\theta_0 > 20$ (Fig. 8), and the reduction in hydraulic conductivity was more significant as θ_0 increased because of increased particle

retention at large values of θ_0 . Note that the results presented in this work are with an assumption of critical velocity [v_c in Eq. (10)] equal to 0.18 cm s^{-1} . (Separation distance is assumed $5.2 \times 10^{-7} \text{ cm}$, corresponding to the distance of kaolinite–water–sand system in 0.1 M monovalent salt solution.) The interparticle attraction forces vary depending on v_c , mineralogy of particles, mineralogy of porous material, and solution chemistry used in the v_c calculation.

As μ_c and σ_c increased, less breakthrough and more significant reduction of K/K_0 were observed due to the significant surface retention of particles (Fig. 6b, c). The majority of particle transport studies and filtration theories have used the median sizes of the particle (exp(μ_c) for lognormal distribution) as the representative size in modeling [3]. However, the results presented in Fig. 7 imply that the mean size of the particle size distribution of particles should be used to model particle transport/retention in porous media because the retention profiles and breakthrough curves are dependent on μ_c as well as σ_c . (The expected value of particle size distribution is exp($\mu_c + \sigma_c^2/2$) for lognormal distribution.)

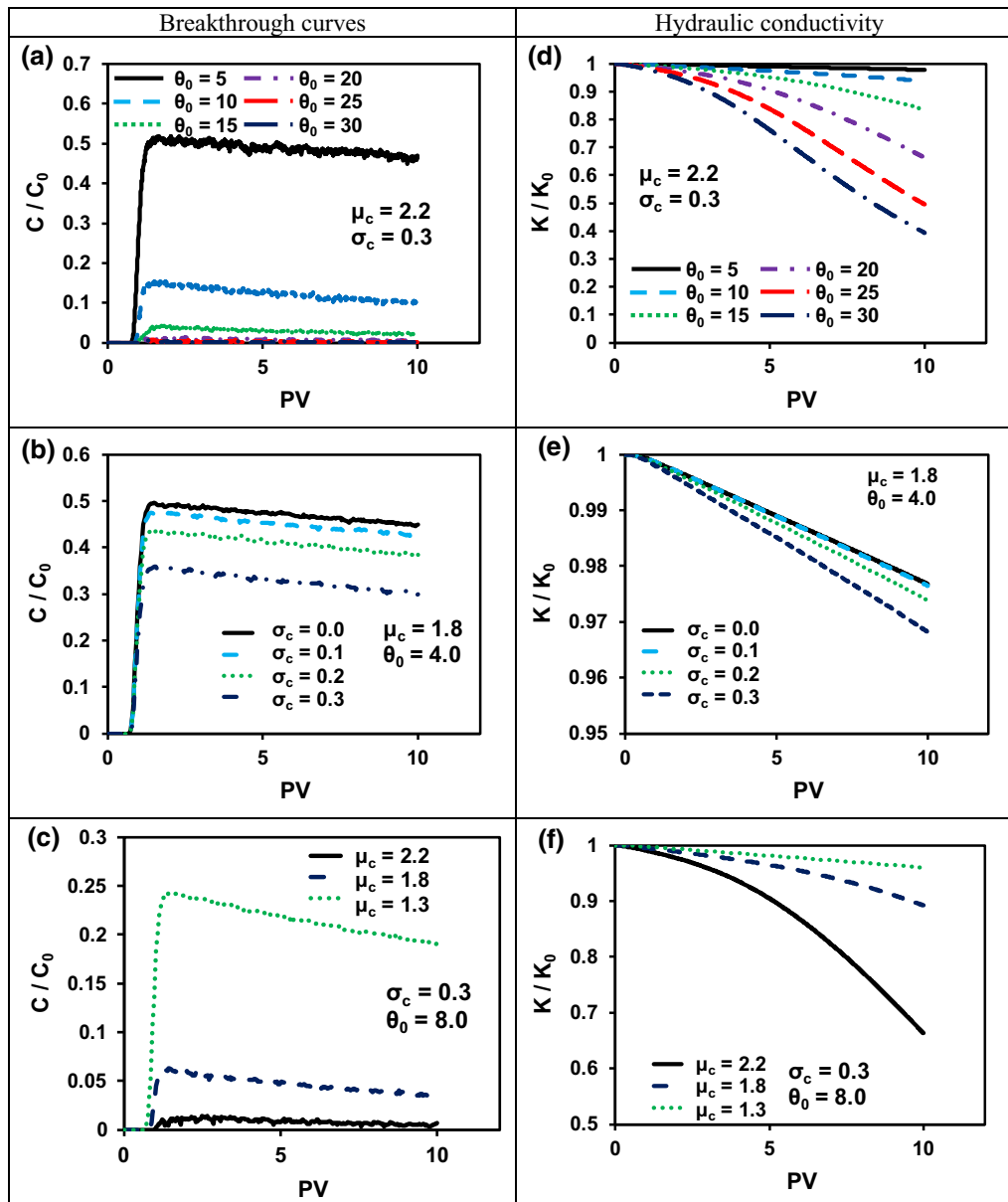


Fig. 8 Breakthrough curves and the reduction in hydraulic conductivity during the injection under varied σ_c at $\mu_c = 1.8$ and $\theta_0 = 4$ (a–c), and under varied $\mu_c = 2.2, 1.8$ and 1.3 at $\theta_0 = 8$ and $\sigma_c = 0.3$ (d–f)

3.3 Size distributions of particles in retention profiles and breakthrough curves

The size distributions of retained particles and effluent particles within the network model were illustrated by box plots (Fig. 9). At low values of interparticle attraction (θ_0), particles were retained uniformly at all depths in sizes that were slightly larger than the median size of the particle size distribution; however, crossover points between median sizes of retained particles and the particle size distribution were observed at relatively high values of interparticle forces (θ_0). This trend of retained particle size under varied θ_0 was comparable for all simulations of mean

particle size (μ_c) and showed that most of the large particles were retained near the injection point (inflow), which led to smaller particles being retained in the bottom part of the sand medium with the impact becoming more significant as θ_0 increased. At low values of θ_0 , the sizes of retained particles were uniformly larger than the median size of the particle size distribution at all depths because of low capture probability. As a result, the median size of effluent particles at $\theta_0 = 2$ was roughly identical with the median size of particles in all pore volumes in the network model. At other θ_0 values, the median sizes of effluent particles were smaller than the median size of the particle size distribution. The difference between the median sizes

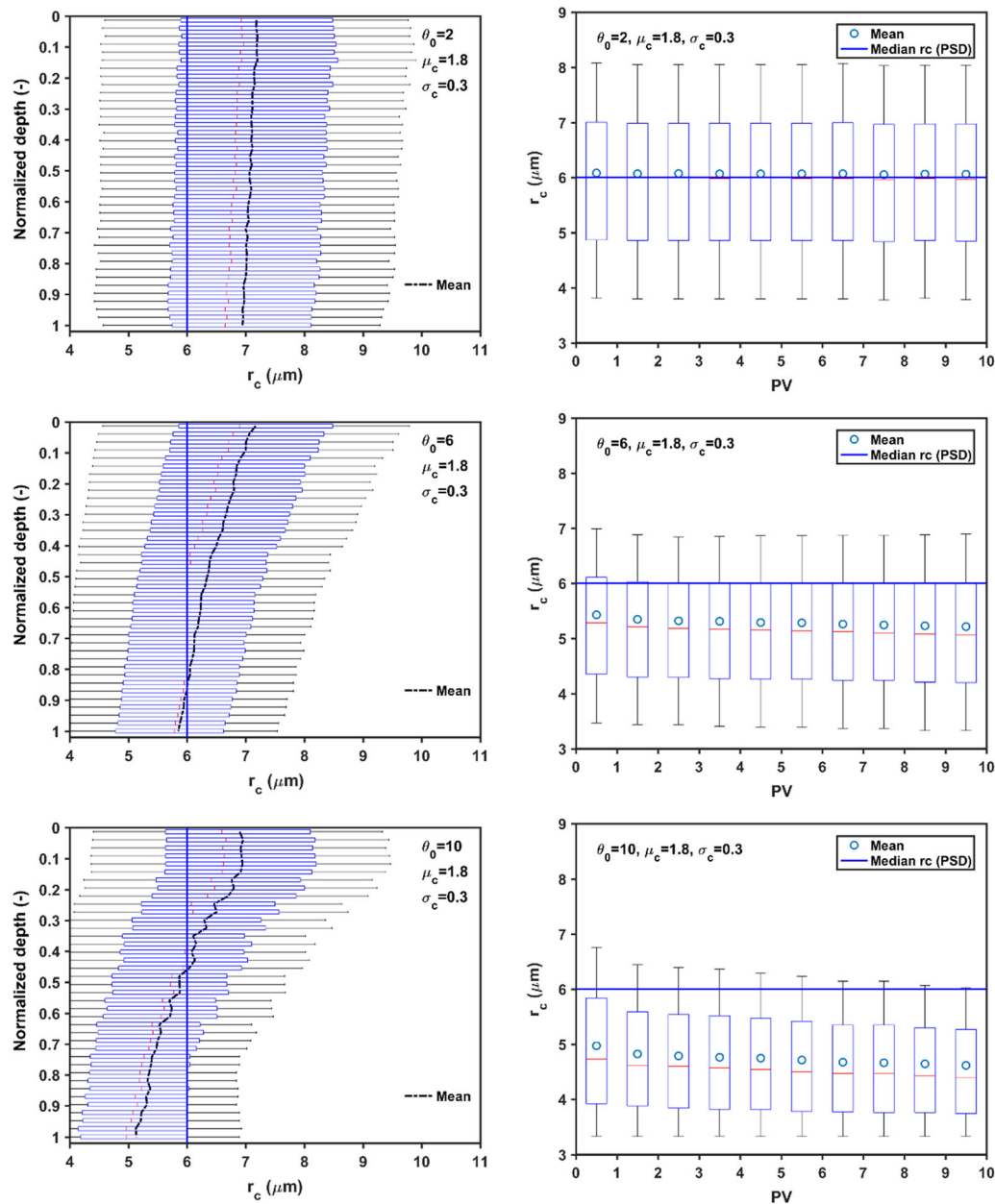


Fig. 9 Size distributions of retained particles and particles in effluent under varied θ_0 at $\mu_c = 1.8$ and $\sigma_c = 0.3$. The edges of the boxes correspond to 25 and 75% coverages, and the red lines in the boxes represent the median value of sizes of retained particles. The whisker line of each box plot indicates 99% coverage for distribution in each depth (color figure online)

of effluent particles and the median (or mean) sizes of the inlet particle distribution was more significant as θ_0 increased (Fig. 9).

4 Conclusions

In this work, a pore network model for polydispersed particle transport in porous media was developed to upscale the pore-scale results into the attachment coefficients in the continuum-scale equation. Based on the

observed retention profiles, breakthrough curves, and the reduction in hydraulic conductivity from the pore network simulation, the following conclusions can be drawn:

1. The pore network model introduced in this work can be used to reflect particle size distribution of the particles, flow rate, and solution chemistry in the estimation of attachment coefficients in the continuum equation for long-term and large-scale simulation.
2. Larger mean and standard deviation of particle size distribution, and a larger interparticle force led to a more significant reduction in hydraulic conductivity,

which is attributed to less breakthrough concentration and a larger amount of retained particles.

3. Low values of interparticle forces resulted in effluent sizes that were similar to the mean of the particle size distribution because the probability of capture (straining or attachment) was low. As the value of the interparticle forces increased, the median sizes of the effluent particles were smaller than the median size of the particle size distribution, with the difference between the median sizes of effluent particles and the median sizes of the particle distribution becoming more significant as θ_0 increased.
4. Further development of the pore network model can reflect other pore-scale characteristics of sand medium (pore-scale geometry, the kinetic energy fluctuations of the particle, degree of saturation) into macroscale parameters such as attachment coefficient.

Acknowledgements This material is based upon work supported by the Georgia Department of Transportation. Any opinions, findings, and conclusions or recommendations expressed in this material are those of the writers and do not necessarily reflect the views of the Georgia Department of Transportation. Special thanks are given to Mr. J.D. Griffith, P.E., P.G. (deceased) for his support of this research project.

References

1. Aghighi M, Hoeh MA, Lehnert W et al (2016) Simulation of a full fuel cell membrane electrode assembly using pore network modeling. *J Electrochem Soc* 163:F384–F392. <https://doi.org/10.1149/2.0701605jes>
2. Auset M, Keller A (2006) Pore-scale visualization of colloid straining and filtration in saturated porous media using micro-models. *Water Resour Res*. <https://doi.org/10.1029/2005WR004639>
3. Bradford SA, Kim H (2010) Implications of cation exchange on clay release and colloid-facilitated transport in porous media. *J Environ Qual* 39:2040. <https://doi.org/10.2134/jeq2010.0156>
4. Bradford SA, Simunek J, Bettahar M et al (2003) Modeling colloid attachment, straining, and exclusion in saturated porous media. *Environ Sci Technol* 37:2242–2250. <https://doi.org/10.1021/es025899u>
5. Bradford SA, Torkzaban S, Simunek J (2011) Modeling colloid transport and retention in saturated porous media under unfavorable attachment conditions. *Water Resour Res*. <https://doi.org/10.1029/2011WR010812>
6. Bradford SA, Torkzaban S, Walker SL (2007) Coupling of physical and chemical mechanisms of colloid straining in saturated porous media. *Water Res* 41:3012–3024. <https://doi.org/10.1016/j.watres.2007.03.030>
7. Bradford SA, Yates SR, Bettahar M, Simunek J (2002) Physical factors affecting the transport and fate of colloids in saturated porous media. *Water Resour Res* 38:63-1–63-12. <https://doi.org/10.1029/2002WR001340>
8. Compère F, Porel G, Delay F (2001) Transport and retention of clay particles in saturated porous media. Influence of ionic strength and pore velocity. *J Contam Hydrol* 49:1–21. [https://doi.org/10.1016/S0169-7722\(00\)00184-4](https://doi.org/10.1016/S0169-7722(00)00184-4)
9. Dai S, Seol Y (2014) Water permeability in hydrate-bearing sediments, a pore scale study. *Geophys Res Lett* 41:4176–4184. <https://doi.org/10.1002/2014GL060535>. Received
10. Delgado JMPQ (2007) Longitudinal and transverse dispersion in porous media. *Chem Eng Res Des* 85:1245–1252. <https://doi.org/10.1205/cherd07017>
11. Gostick J, Aghighi M, Hinebaugh J et al (2016) OpenPNM: a pore network modeling package. *Comput Sci Eng* 18:60–74. <https://doi.org/10.1109/MCSE.2016.49>
12. Gu DM, Huang D, Liu HL et al (2019) A DEM-based approach for modeling the evolution process of seepage-induced erosion in clayey sand. *Acta Geotech* 14:1629–1641
13. Hajra MG, Reddi LN, Glasgow LA et al (2002) Effects of ionic strength on fine particle clogging of soil filters. *J Geotech Geoenviron Eng* 128:631–639. [https://doi.org/10.1061/\(ASCE\)1090-0241\(2002\)128:8\(631\)](https://doi.org/10.1061/(ASCE)1090-0241(2002)128:8(631))
14. Happel J, Brenner H (2012) *Low Reynolds number hydrodynamics: with special applications to particulate media*, 1st edn. Springer, Berlin
15. Harvey RW, Garabedian SP (1991) Use of colloid filtration theory in modeling movement of bacteria through a contaminated sandy aquifer. *Environ Sci Technol* 25:178–185. <https://doi.org/10.1021/es00013a021>
16. Hu Z, Zhang Y, Yang Z (2019) Suffusion-induced deformation and microstructural change of granular soils: a coupled CFD–DEM study. *Acta Geotech* 14:795–814
17. Imdakm AO, Sahimi M (1991) Computer simulation of particle transport processes in flow through porous media. *Chem Eng Sci* 46:1977–1993. [https://doi.org/10.1016/0009-2509\(91\)80158-U](https://doi.org/10.1016/0009-2509(91)80158-U)
18. Israelachvili JN (2011) *Intermolecular and surface forces: revised, 3rd edn*. Academic press, London
19. Kuznar ZA, Elimelech M (2007) Direct microscopic observation of particle deposition in porous media: role of the secondary energy minimum. *Colloids Surf A Physicochem Eng Asp* 294:156–162. <https://doi.org/10.1016/j.colsurfa.2006.08.007>
20. Litton GM, Olson TM (1996) Particle size effects on colloid deposition kinetics: evidence of secondary minimum deposition. *Colloids Surf A Physicochem Eng Asp* 107:273–283. [https://doi.org/10.1016/0927-7757\(95\)03343-2](https://doi.org/10.1016/0927-7757(95)03343-2)
21. Luo Y, Huang Y (2020) Effect of open-framework gravel on suffusion in sandy gravel alluvium. *Acta Geotech*. <https://doi.org/10.1007/s11440-020-00933-9>
22. Luo Y, Luo B, Xiao M (2019) Effect of deviator stress on the initiation of suffusion. *Acta Geotech* 15:1607–1617. <https://doi.org/10.1007/s11440-019-00859-x>
23. Mackie RI, Horne RMW, Jarvis RJ (1987) Dynamic modeling of deep-bed filtration. *AIChE J* 33:1761–1775. <https://doi.org/10.1002/aic.690331102>
24. McCarthy JF, Zachara JM (1989) Subsurface transport of contaminants. *Environ Sci Technol* 23:496–502. <https://doi.org/10.1021/es00063a001>
25. Nguyen CD, Benahmed N, Andò E et al (2019) Experimental investigation of microstructural changes in soils eroded by suffusion using X-ray tomography. *Acta Geotech* 14:749–765
26. Pirnia P, Duhaime F, Ethier Y, Dubé J-S (2020) Hierarchical multiscale numerical modelling of internal erosion with discrete and finite elements. *Acta Geotech*. <https://doi.org/10.1007/s11440-020-01009-4>
27. Raouf A, Nick HM, Hassanizadeh SM, Spiers CJ (2013) Pore-Flow: a complex pore-network model for simulation of reactive transport in variably saturated porous media. *Comput Geosci* 61:160–174. <https://doi.org/10.1016/j.cageo.2013.08.005>
28. Reddi LN, Xiao M, Hajra MG, Lee IM (2005) Physical clogging of soil filters under constant flow rate versus constant head. *Can Geotech J* 42:804–811. <https://doi.org/10.1139/t05-018>

29. Rege SD, Fogler HS (1988) A network model for deep bed filtration of solid particles and emulsion drops. *AIChE J* 34:1761–1772. <https://doi.org/10.1002/aic.690341102>
30. Schijven JF, Hassanizadeh SM (2000) Removal of viruses by soil passage: overview of modeling, processes, and parameters. *Crit Rev Environ Sci Technol* 30:49–127. <https://doi.org/10.1080/10643380091184174>
31. Tranter TG, Gostick JT, Burns AD, Gale WF (2016) Pore network modeling of compressed fuel cell components with OpenPNM. *Fuel Cells* 16:504–515. <https://doi.org/10.1002/fuce.201500168>
32. Valvatne PH, Piri M, Lopez X, Blunt MJ (2005) Predictive pore-scale modeling of single and multiphase flow. In: Das D, Hassanizadeh S (eds) *Upscaling multiphase flow in porous media*. Springer, Dordrecht, pp 23–41
33. Won J, Burns SE (2017) Influence of ionic strength on clay particle deposition and hydraulic conductivity of a sand medium. *J Geotech Geoenviron Eng* 143:04017081. [https://doi.org/10.1061/\(ASCE\)GT.1943-5606.0001780](https://doi.org/10.1061/(ASCE)GT.1943-5606.0001780)
34. Xiong Q, Baychev TG, Jivkov AP (2016) Review of pore network modelling of porous media: experimental characterisations, network constructions and applications to reactive transport. *J Contam Hydrol* 192:101–117. <https://doi.org/10.1016/j.jconhyd.2016.07.002>
35. Yang J, Yin Z-Y, Laouafa F, Hicher P-Y (2019) Modeling coupled erosion and filtration of fine particles in granular media. *Acta Geotech* 14:1615–1627
36. Yuan H, Shapiro A, You Z, Badalyan A (2012) Estimating filtration coefficients for straining from percolation and random walk theories. *Chem Eng J* 210:63–73. <https://doi.org/10.1016/j.cej.2012.08.029>
37. Zhang F, Damjanac B, Huang H (2013) Coupled discrete element modeling of fluid injection into dense granular media. *J Geophys Res Solid Earth* 118:2703–2722. <https://doi.org/10.1002/jgrb.50204>

Publisher's Note Springer Nature remains neutral with regard to jurisdictional claims in published maps and institutional affiliations.